European Rotorcraft Forum

A NEW APPROACH FOR FINITE STATE DYNAMIC ROTOR INFLOW MODELLING

Raphaël Perret, raphael.perret@onera.fr, ONERA, DTIS (France)
Pierre-Marie Basset, pierre-marie.basset@onera.fr, ONERA, DTIS (France)
Jean-Marc Moschetta, jean-marc.moschetta@isae-supaero.fr, ISAE-SUPAERO, Université de Toulouse, (France)

Abstract
We present a new method to model the induced velocities generated by a rotor. A spectral Galerkin method is applied to the incompressible non linear Euler equations, and filters are added to improve stability, while maintaining the accuracy of the scheme. We then compare it to other induced velocity models with satisfying results, while underlying some further work.

1. INTRODUCTION

For rotary wings aircraft, the induced velocities by the rotors have significant impacts on the rotor blades themselves and on the aerodynamics of the other rotorcraft elements by interferences (e.g. the tail components: horizontal and vertical stabilizers, tail rotor etc.). Therefore, the modelling of the whole rotor induced velocity field (on and off the rotor) with a unified dynamic model scalable to each simulation application from presizing to flight dynamics is a crucial topic. In this paper we present the development of a new induced velocity model for rotors, with an actuator disk. This model is inspired by the work of Peters and Huang [1], but takes a quite different path in order to offer a model build on less restrictive assumptions. This model requires neither the linearization of the momentum conservation equation, nor the assumption of a velocity potential and respect the continuity equation in all the domain. Thus it provides the values of the induced velocities at all points on and around the rotor in a homogeneous way.

Modelling the induced velocities of an actuator disk has been a subject of study for more than 50 years, with, among others, Amer [2]. One of the main contributor to this subject is D. Peters which has developed several models, beginning with the Pitt and Peters model [3], to the recent model presented in [1]. Other models have been developed using different approaches, like Conway [4] who provided an analytic study of the actuator disk, or more numerical like Le Chuiton [5] who coupled an actuator disk model to a finite element method, or [6] who compared various actuator disk representations also with a finite element method. However none of those approaches takes full advantages of the efficiency of a spectral method as Peters' method, which can be a severe drawback for numerous applications, as demonstrated by Peters in [7].

For this new method, the incompressible nonlinear Euler equations are dealt with a spectral approach highly inspired by the work of Lopez, Marques and Shen [8]. However several modifications have to be made in order to fit their method to our application. The various modifications are required by the fact that, in our application, viscosity is negligible, which tends to prevent its natural damping effect on the equations, and by the fact that we deal with a severely truncated open domain. Otherwise the same steps are taken to solve the equations: we approximate the velocity and pressure by families of Legendre's polynomials which respect the chosen boundary conditions, and solve explicitly the velocity coefficients (inflow states), with a second order pressure projection scheme allowing to maintain the continuity equation. Furthermore the nonlinear terms are treated explicitly, and approximated by Gauss-Legendre-Lobatto quadrature.

First we will underline the motivation for this new method, then the algorithm will be presented. After a presentation of the way the rotor is accounted for, we will present the approximation chosen and the various filters used. Two types of filters are used: on the input of the model, in order to reduce the effect of the Gibbs phenomenon due to the discontinuity of our blade airloads inputs, and on the states, in order to maintain the stability of the scheme, which is threaten by the high order terms developed by

the nonlinear terms. Finally we present examples of results of transition flight and descending flight in order to demonstrate the capabilities of the new model.

2. MOTIVATION

The aim of this new model is to keep the advantages present in Peters and Huang model while surpassing drawbacks due to some limiting assumptions. One of the major strength of the finite states formulation is its capacity of adaptation to all applications through the choice of the number of coefficients in the approximation (inflow states). Indeed its finite states formulation allows to adapt to the need of each practical application with a trade-off between the speed of the computation and its accuracy in the fineness of the inflow field description. For example, it can be used for real-time flight dynamics simulation and conception loops for the predesign of rotorcraft thanks to its computational efficiency with a reasonable number of inflow states tailored to needs of these applications. With a higher truncation, it tends to provide a description of the induced field close to the ones given by more costly models such as free wake models. Moreover, this finite states approach is more suited for application requiring clear defined states such as aeroelasticity (e.g. Floquet method) and any application requiring linearization, identification. It does however have a few drawbacks, that this new model aims to surpass.

After a study of Peters and Huang model, as well as its predecessors, it became apparent that the bulk of the advantages of this model comes from the use of a spectral Galerkin method, while the drawbacks take their origins in the restrictive assumptions taken in order to apply the Galerkin method to the Euler equations.

Thus, the main part of the development of the proposed new model has been accomplished by removing some assumptions taken by Peters and Huang, in order to avoid the latter drawbacks they would generate, while still applying a Galerkin method to the equations.

We here list the assumptions taken in our new model which are also taken by Peters and Huang model, then the ones taken only by Peters and Huang model and their consequences on the representation of the induced velocity field.

From the Navier-Stokes equations, the only additional assumptions are the incompressibility and the negligible viscosity of the rotor flow. One can justify both assumptions by limiting the validity of the model to high Reynolds number and to the low Mach number of the induced velocity. Thus with those two assumptions the Navier-Stokes equations are reduced to the incompressible Euler equations. The Peters and Huang model makes a series of extra assumptions. First they linearize the non linear terms. This has a number of consequences. Firstly, it implies the introduction of two static parameters, V_∞ and χ, the module of the freestream velocity and the wake skew angle. Secondly, it considers that the induced velocities will be negligible compared to the freestream velocity, which makes the hover case a limiting case. Finally, it makes the evolution of the velocities in the wake unnatural when modifying the wake angle, by making the streamtube of induced velocities moves as a block. Another assumption of their approach is the velocity potential assumption. Although this might be justified above the rotor, one can not consider the flow below the rotor as irrotational. This create an asymmetry in the treatment of the upstream and downstream part of the domain, leading to the introduction of a peculiar case for all velocities below the rotor, and making all the descend cases difficult to represent. Finally, the Peters and Huang model is formulated in the frequency domain. This allows to solve the equations only once in order to obtain the whole time history of the induced velocity. However, in practical applications, the induced velocity models are always linked to a blade element model allowing to provide inputs (mainly in the form of rotor airloads). Therefore, a time domain formulation of the model would be better appreciated. Adapting the frequency formulation to a time formulation can be done, but generates new problems. Indeed, while solving for the velocities below the rotor, Peters and Huang model heavily relies on the frequency formulation. This leads to the need to access values of the velocities at various times, depending on where one wants the velocities, and also at times that are not yet computed, in some cases.

In the following sections a short insight of the new proposed method for solving the incompressible Euler equations in the presence of a rotor will be given, as well as some examples.

3. METHODOLOGY

3.1. Domain

Although the ellipsoidal coordinate system used by Peters et al. is perfectly suited to represent the airflow through a rotor, and could be a way to improve the current model, its inherent singularities are causing convergence problems, notably at the edge of the disk. In order to avoid them, the cylindrical coordinate system was chosen. It also presents a singularity on the axis, but its regularisation has been studied

in numerous papers (see Ref [8, 9, 10]). Therefore the computational domain is defined as a cylinder Ω of aspect ratio Λ with a rotor at its center, as presented in Fig 1. It can be described as follows:

$$\Omega = \{0 \leqslant \overline{r} \leqslant R, 0 \leqslant \theta < 2\pi, -\frac{H}{2} \leqslant \overline{z} \leqslant \frac{H}{2}\} \tag{1}$$

with R its radius, and H its height, and therefore $\Lambda = \frac{H}{R}$.

Furthermore, in order to use Legendre polynomials, the $\overline{r}$ and $\overline{z}$ coordinates are rescaled in $[-1; 1]$ with:

$$x = \frac{2\overline{r}}{R} - 1 \tag{2}$$

$$z = \frac{2\overline{z}}{H} \tag{3}$$

We will also use $r = \frac{x+1}{2}$.

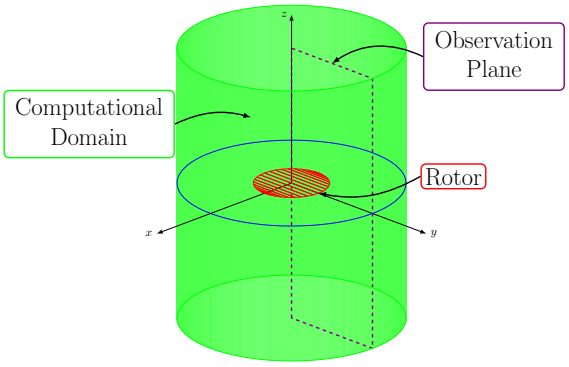

Figure 1: Representation of the computational domain

3.2. Assumptions and equations

The Navier-Stokes equations governing the flow are considered under the following assumptions. The airflow is considered to be incompressible and the viscosity to be negligible, because of the high Reynolds numbers of our applications. The boundary conditions will be detailed in section 3.4. Therefore the following general form of the incompressible Euler equations are dealt with:

$$\begin{aligned} \frac{\partial \overrightarrow{V}}{\partial t} + \overrightarrow{\nabla}(\overrightarrow{V}) \cdot \overrightarrow{V} &= \overrightarrow{\nabla} p \\ \nabla \cdot \overrightarrow{V} &= 0 \end{aligned} \tag{4}$$

We set $u^+ = u + iv$ and $u^- = u - iv$ following Ref [8]. This gives the final form of the equations, in the cylindrical system, shown in equation 5 (see next page).

Finally, one can already account for the Fourier series expansion in azimuth in order to distinguish between the different orders, for a given time step k:

$$u_k^+(x, \theta, z) = \sum_{m=-N_\theta}^{N_\theta} u_{k,m}^+(x, z) e^{im\theta} \tag{6}$$

$$u_k^-(x, \theta, z) = \sum_{m=-N_\theta}^{N_\theta} u_{k,m}^-(x, z) e^{im\theta} \tag{7}$$

$$w_k(x, \theta, z) = \sum_{m=-N_\theta}^{N_\theta} w_{k,m}(x, z) e^{im\theta} \tag{8}$$

$$p_k(x, \theta, z) = \sum_{m=-N_\theta}^{N_\theta} p_{k,m}(x, z) e^{im\theta} \tag{9}$$

3.3. Time discretization

Following the development made in Ref. [11, 8], a second order projection scheme is used. For the reader's convenience, we expose here the general principles of the time discretization scheme.

The first step of the scheme, at time step k and for a given order m, is:

$$\begin{aligned} \frac{1}{2\delta_t}\left(3\overrightarrow{v}_{k+1,m} - 4\overrightarrow{v_{k,m}} + \overrightarrow{V}_{k-1,m}\right) = \\ -\overrightarrow{\nabla} p_{k,m} - 2\overrightarrow{N}_{k,m} + \overrightarrow{N}_{k-1,m} \end{aligned} \tag{10}$$

where $\overrightarrow{v}_{k+1,m}$ is an estimation of the velocity at time step $k+1$. The non linear terms are treated explicitly by using a simple backward scheme with their known values at time step k, $\overrightarrow{N}_{k,m}$ and $k-1$, $\overrightarrow{N}_{k-1,m}$.

This thus gives:

$$\frac{3}{2\delta_t}(\overrightarrow{V}_{k+1,m} - \overrightarrow{v}_{k+1,m}) = -\overrightarrow{\nabla}(p_{k+1,m} - p_{k,m}) \tag{11}$$

Using the continuity equation one can find the value of the pressure term p_{k+1}:

$$-\frac{3}{2\delta_t}\nabla \cdot (\overrightarrow{v}_{k+1,m}) = -\Delta(p_{k+1,m} - p_{k,m}) \tag{12}$$

And thus compute the value of the velocity at $k+1$

$$
\begin{aligned}
&\frac{\partial u^+}{\partial t}+\frac{u^+ + u^-}{2}\frac{\partial u^+}{\partial r}+\frac{u^+ - u^-}{2ir}\left(\frac{\partial u_+}{\partial \theta}+iu_+\right)+w\frac{\partial u^+}{\partial z} &&= \frac{\partial p}{\partial r}\\
&\frac{\partial u^-}{\partial t}+\frac{u^+ + u^-}{2}\frac{\partial u^-}{\partial r}+\frac{u^+ - u^-}{2ir}\left(\frac{\partial u_-}{\partial \theta}-iu_-\right)+w\frac{\partial u^-}{\partial z} &&= \frac{\partial p}{r\partial \theta}\\
&\frac{\partial w}{\partial t}+\frac{u^+ + u^-}{2}\frac{\partial w}{\partial r}+\frac{u^+ - u^-}{2i}\frac{\partial w}{r\partial \theta}+w\frac{\partial w}{\partial z} &&= \frac{\partial p}{\partial z}\\
&\frac{\partial}{r\partial r}\left(r\frac{u^+ + u^-}{2}\right)+\frac{\partial}{r\partial \theta}\left(\frac{u^+ - u^-}{2i}\right)+\frac{\partial w}{\partial z} &&= 0
\end{aligned}
\tag{5}
$$

with equation 11:

$$
\overrightarrow{v}_{k+1,m} = \overrightarrow{\tilde{v}}_{k+1,m} - \frac{2\delta_t}{3}\overrightarrow{\nabla}(p_{k+1,m} - p_{k,m}) \tag{13}
$$

It can be noticed that the use of the continuity equation ensure that the velocity has no divergence in the whole domain (thus ensuring the respect of the continuity equation both above and below the rotor), and that the explicit treatment of the non linear terms will highly simplify their integration to the Galerkin method.

3.4. Boundary conditions

The boundary conditions imposed are of two types. On the boundaries of the cylindrical domain, open boundary conditions are chosen. Two different possibilities for those boundary conditions have been tested. The first is a boundary condition developed by Dong in Ref. [12]. It allows vortices to leave the domain without causing divergence, by compensating the energy with a pressure term. The second one is merely a Neumann boundary condition on the pressure which allows to maintain stability. The Neumann boundary condition was finally retain for its ease of implementation in the context of a spectral method.

On the axis, regularity boundary conditions, called pole conditions, must be imposed in order to have a valid solution. As mentioned by Lopez et al. in Ref. [8], one can distinguish two sets of pole conditions to be imposed on the axis: the essential pole conditions, that are the minimal requirement for the velocity to be regular, and the natural pole conditions that ensure analicity in the cartesian coordinates system. In the current version of the model, only the essential pole conditions are accounted for. Although the issue is still under investigation, not accounting for the natural pole conditions leads to irregularities on the axis in the high advance ratio cases, which is probably due to the hyperbolic nature of our equations. One way to solve this issue would be to account for all the pole conditions following the method presented in Ref. [10].

The chosen boundary conditions in $x = \pm 1$ ($x = -1$ on the axis and $x = 1$ at the edge of the domain) depend on the azimuthal order because of the pole conditions. Therefore we have, for $m = 0$:

$$
\left.\frac{\partial u^+_{k,0}}{\partial x}\right|_{x=\pm 1} = 0 \quad \text{and} \quad u^+_{k,0}(x=-1) = 0 \tag{14}
$$

$$
\left.\frac{\partial w_{k,0}}{\partial x}\right|_{x=\pm 1} = 0 \tag{15}
$$

$$
\left.\frac{\partial p_{k,0}}{\partial x}\right|_{x=\pm 1} = 0 \tag{16}
$$

For $m = 1$:

$$
\left.\frac{\partial u^+_{k,1}}{\partial x}\right|_{x=\pm 1} = 0 \quad \text{and} \quad u^+_{k,1}(x=-1) = 0 \tag{17}
$$

$$
\left.\frac{\partial u^-_{k,1}}{\partial x}\right|_{x=\pm 1} = 0 \tag{18}
$$

$$
\left.\frac{\partial w_{k,1}}{\partial x}\right|_{x=\pm 1} = 0 \quad \text{and} \quad w_{k,1}(x=-1) = 0 \tag{19}
$$

$$
\left.\frac{\partial p_{k,1}}{\partial x}\right|_{x=\pm 1} = 0 \quad \text{and} \quad p_{k,1}(x=-1) = 0 \tag{20}
$$

For $m > 1$:

$$
\left.\frac{\partial u^+_{k,m}}{\partial x}\right|_{x=\pm 1} = 0 \quad \text{and} \quad u^+_{k,m}(x=-1) = 0 \tag{21}
$$

$$
\left.\frac{\partial u^-_{k,m}}{\partial x}\right|_{x=\pm 1} = 0 \quad \text{and} \quad u^-_{k,m}(x=-1) = 0 \tag{22}
$$

$$
\left.\frac{\partial w_{k,m}}{\partial x}\right|_{x=\pm 1} = 0 \quad \text{and} \quad w_{k,m}(x=-1) = 0 \tag{23}
$$

$$
\left.\frac{\partial p_{k,m}}{\partial x}\right|_{x=\pm 1} = 0 \quad \text{and} \quad p_{k,m}(x=-1) = 0 \tag{24}
$$

And finally the boundary conditions in z, for all m:

$$\left.\frac{\partial \overrightarrow{v}_{k,m}}{\partial z}\right|_{z=\pm 1} = 0 \tag{25}$$

$$\left.\frac{\partial p_{k,m}}{\partial z}\right|_{z=\pm 1} = 0 \tag{26}$$

3.5. Spectral Method

In order to solve the equations at each time step, a spectral Galerkin method is applied on the equations. This allows the same advantages as the ones of the Huang and Peters model to be maintained. However, we follow Lopez, Marques and Shen (Ref. [8]) for the choice of the approximation space, contrived by the chosen boundary conditions. Because of the essential pole conditions imposed on the axis, the description of the velocity depends on the azimuthal order considered. Nevertheless, there will always be N_r and N_z elements for the radial and axial descriptions respectively. Furthermore, the time index, noted k previously, has been dropped for the sake of clarity.

For $m = 0$:

$$u_0^+(x,z) = \sum_{j=0}^{N_j-1}\sum_{n=0}^{N_r-1} \hat{u}_{0,j}^{+,n}\kappa_n(x)\gamma_j(z) \tag{27}$$

$$u_0^-(x,z) = \sum_{j=0}^{N_j-1}\sum_{n=0}^{N_r-1} \hat{u}_{0,j}^{-,n}\kappa_n(x)\gamma_j(z) \tag{28}$$

$$w_0(x,z) = \sum_{j=0}^{N_j-1}\sum_{n=0}^{N_r-1} \hat{w}_{0,j}^{n}\gamma_n(x)\gamma_j(z) \tag{29}$$

$$p_0(x,z) = \sum_{j=0}^{N_j-1}\sum_{n=0}^{N_r-1} \hat{p}_{0,j}^{n}\gamma_n(x)\gamma_j(z) \tag{30}$$

For $m = 1$:

$$u_1^+(x,z) = \sum_{j=0}^{N_j-1}\sum_{n=0}^{N_r-1} \hat{u}_{1,j}^{+,n}\kappa_n(x)\gamma_j(z) \tag{31}$$

$$u_1^-(x,z) = \sum_{j=0}^{N_j-1}\sum_{n=0}^{N_r-1} \hat{u}_{1,j}^{-,n}\gamma_n(x)\gamma_j(z) \tag{32}$$

$$w_1(x,z) = \sum_{j=0}^{N_j-1}\sum_{n=0}^{N_r-1} \hat{w}_{1,j}^{n}\kappa_n(x)\gamma_j(z) \tag{33}$$

$$p_1(x,z) = \sum_{j=0}^{N_j-1}\sum_{n=0}^{N_r-1} \hat{p}_{1,j}^{n}\kappa_n(x)\gamma_j(z) \tag{34}$$

For $m > 1$:

$$u_m^+(x,z) = \sum_{j=0}^{N_j-1}\sum_{n=0}^{N_r-1} \hat{u}_{m,j}^{+,n}\kappa_n(x)\gamma_j(z) \tag{35}$$

$$u_m^-(x,z) = \sum_{j=0}^{N_j-1}\sum_{n=0}^{N_r-1} \hat{u}_{m,j}^{-,n}\kappa_n(x)\gamma_j(z) \tag{36}$$

$$w_m(x,z) = \sum_{j=0}^{N_j-1}\sum_{n=0}^{N_r-1} \hat{w}_{m,j}^{n}\kappa_n(x)\gamma_j(z) \tag{37}$$

$$p_m(x,z) = \sum_{j=0}^{N_j-1}\sum_{n=0}^{N_r-1} \hat{p}_{m,j}^{n}\kappa_n(x)\gamma_j(z) \tag{38}$$

The definition of the polynomials chosen can be found $\forall n \in \mathbb{N}$ in equation 39 (see next page). We use L_n to represent the n^{th} Legendre polynomial.

They ensure the boundary conditions thanks to the following properties, $\forall n \in \mathbb{N}$:

$$\frac{\partial \gamma_n}{\partial x}(\pm 1) = 0 \tag{40}$$

$$\kappa_n(-1) = 0 \quad \text{and} \quad \frac{\partial \kappa_n}{\partial x}(\pm 1) = 0 \tag{41}$$

Finally, applying the same method as described in Ref. [13, 8], one can solve efficiently for the coefficients and reconstruct an approximation of the velocity as precise as necessary by choosing the order of the approximations N_r, N_z and N_θ.

3.6. Non linear terms

The convection terms in the momentum conservation equation are not linearized in the proposed approach, but dealt with a Gauss-Legendre-Lobatto quadrature. As mentioned, this avoids the description of the rotor airflow by rectilinear streamlines and a wake skew angle, making the airflow move rigidly with the variations of the wake angle. The new model allows to account for the rotor wake deformation during transition and maneuvering flights, thus preventing the need of special additional treatment for wake distortion.

However these non-linear terms are causing some issues. They can contribute to the divergence of the algorithm and to some irregularities. Indeed, the most obvious examples being the orthoradial derivative terms that are divided by r. Those terms imply a loss of regularity on the axis, unless the velocity respects some pole conditions. The study of a full satisfactory treatment of these non-linear terms is on-going although satisfying results are already obtained as will be shown in section 5. Therefore their

$$\begin{aligned}\gamma_n(x) &= L_n(x) - \frac{n(n+1)}{(n+2)(n+3)} L_{n+2}(x) \\ \kappa_n(x) &= -\frac{n^2+5n+6}{n+1} L_n(x) - \frac{2n^3+17n^2+45n+36}{(2n+5)(n+1)} L_{n+1}(x) + nL_{n+2}(x) + \frac{2n^2+7n+6}{2n+5} L_{n+3}\end{aligned} \tag{39}$$

detailed treatment will not be exposed in this paper.

4. APPLICATION TO A ROTOR

4.1. Definition of the rotor

There are numerous ways to model a rotor in a flow. Our point of view will be to see it as an actuator disk, changing the point of view Peters et al. had in numerous models (Ref. [14, 15, 16]), where the effect of the rotor was seen as a discontinuity of pressure across the rotor. Seeing the actuator disk as a discontinuity of pressure has for consequences to cut the domain and to impose the effect of the rotor as a pressure boundary condition. This is an issue, since the velocity boundary conditions at the cut of the domain, i.e. in the plane of the rotor and on the rotor itself, are unknown. Furthermore, in the cylindrical coordinate system such a discontinuity is not embedded in the coordinates, as it is in the ellipsoidal coordinates system, and would be entirely artificial. This led us to search for a better alternative.

A good review of the various actuator disk models in use can be found in Ref. [5] by Le Chuitton. In his paper, one can see that a good alternative used in computational fluid dynamics is to see the actuator disk effect as source terms which can be readily added to the momentum conservation equation. Furthermore, seeing the effect of the rotor as well-placed density forces has several advantages: it allows for a direct transcription of what is known in the blade model (i.e. the forces on the blades), and allows a less constrained form of input than if expressed under the form of a pressure gradient (calculated from the rotor lift distribution). Furthermore, this point of view allows to take into account more than one rotor in the domain, by simply adding more sources, which could be of interest, notably in the case of co-axial rotors. Finally, the description of those forces can be as precise as wanted, in the same manner as with a pressure discontinuity.

There is however one drawback to this vision of the rotor when used within a spectral method: this description will lead to discontinuities, or at least high gradients, that will generate Gibbs phenomena. Indeed, considering the rotor as infinitely thin compared to the domain size will lead to a sharp function for the representation of the forces applied by the rotor. We will address this concern in the next section.

4.2. Stability and accuracy

Because of the hyperbolic nature of the incompressible Euler equations, and the sharp nature of our inputs, the numerical stability of the algorithm is not guaranteed. The question of the long time stability of those equations has no obvious answer (see Ref. [17] for addressing this issue and a comparison with the Navier-Stokes equations stability), and Gibbs phenomena can easily contaminate the results of a simulation. However, several methods have been developed in order to deal with this inconveniences. Among the most efficient and accurate ones, filters are the easiest to integrate to a spectral method. They have been thoroughly defined in Ref. [18], and proposed in Ref. [19] as a solution for stability issues of spectral methods. Furthermore, the application of filters in Legendre spectral method has been studied with encouraging results most notably in Ref. [20].

In our application two types of filters are used, one for accuracy and one for stability.

4.2.1. Filtering for accuracy

The inputs of this algorithm are the projection of the aerodynamic forces generated by the rotor blades on the chosen approximation space. Because of the rotor geometry, the representation of the forces is concentrated on a small part of the domain, even more so with an actuator disk.

As underlined previously, filtering the inputs is not a necessity, but might highly improve the convergence rate of the algorithm. The main problem in the representation of the inputs are their sharp shapes. This will lead to the apparition of the well-known Gibbs phenomenon, even if the input is not strictly discontinuous. The phenomenon will appear both in the axial direction (due to the thin rotor) and in the radial direction (due to the rapid transition from on the disk to off the disk at the blade tip).

The literature on the treatment of the Gibbs phenomenon is extensive and contains numerous various solutions. We have here taken the party to filter the inputs in order to mitigate the effect of the spurious modes. Furthermore, instead of considering

an infinitely thin rotor, we have considered an arbitrary thickness and smoothed the application of the forces with a gaussian function.

Those choices led us to favour the stability far from the discontinuity at the cost of the accuracyon the disk, by choosing a Lanczos filter σ_L of the form:

$$\sigma_L(\eta) = \frac{\sin(\pi\eta)}{\pi\eta} \quad (42)$$

where η is a variable in $[0, 1]$ representing the order of the coefficients considered.

This filter significantly dampens the impact of the Gibbs phenomenon on the inputs of the algorithm. As can be seen on Fig. 2, the filtered inputs present far less artifacts than the unfiltered one, while representing accurately the input. It is to be noticed that this is at the cost of the accuracy of the representation around $x = 0$, where the value of the input is not reach, and the support of the function is too large. However the overall pointwise accuracy of the filtered approximations is significantly better. The Lanczos filter is a good compromise between significantly damping the oscillations and being accurate.

4.2.2. Filtering for stability

In order to maintain stability, a filter has to be applied on the coefficients of the velocity at each time step. As mentioned in Ref. [21], the impact of such an approach will imply a much stronger cumulative effect of the filter than the one of the filter applied only once. Furthermore, the effect of a filter may be interpreted as adding some viscosity to the equations as mentioned in Ref. [20]. However, Ref. [20] does also show that the filter (under certain requirements) does not alter the converged solution. This led us to choose for an adaptable filter, allowing us to modulate between the damping introduced by the filter and the limitation of the divergent behaviour of the equations, while still being able to give satisfying solutions.

This leads to the following choice of filter for this application, often found in the literature:

$$\sigma_p(\eta) = \exp\left(-\alpha\eta^{2p}\right) \quad (43)$$

Where p is an integer defining the order of the filter and $\alpha = -log(\epsilon)$ (where ϵ is the machine zero).

4.3. Efficiency

There are two main steps in the algorithm. First compute the non linear terms coefficients from the previous step with a Legendre-Gauss-Lobatto quadrature, then compute the new velocity coefficients for the current time, with the time scheme presented above.

One of the first strategies used in order to improve the efficiency of the algorithm is the use of the matrix decomposition method as described in Ref. [13]. This allows to separate the axial and radial coefficients in order to only deal with matrices of size $N_r * N_r$ and $N_z * N_z$ rather than $(N_r + N_z) * (N_r + N_z)$. This allows a great improvement for all matrices multiplications and inversions. A second strategy would be the parallelisation of the algorithm. Indeed, the computation of the non linear terms could highly benefit from such an improvement, and, in the second step, since all azimuthal orders are independent, they could be processed in parallel.

A final aspect of this spectral method is the fact that the inputs given by the rotor have to be adapted for the model. This has the consequence of demanding additional computational effort at each time step due to the translation of the spatial data into spectral ones. This could be reduced by the use of a spectral blade element model, but to the knowledge of the authors, no such models exist yet.

5. RESULTS

In this section examples of results are presented. First we compare the new model to the Huang and Peters model which has been our reference during the process of developing this new model. In a second time, the capabilities of the new model are illustrated on two cases that demonstrate its interest compared to the Huang and Peters model. Finally the model is compared with a prescribed wake model in the case of a two bladed rotor.

5.1. Comparisons to Huang and Peters Model

The comparisons between the results given by the Huang and Peters model and those obtained with the proposed model are not straightforward. The main struggle in order to compare the two models accurately is to be able to generate inputs having the same effect. To do so, we use a classical input for the Huang and Peters model, which represents an axisymmetric pressure discontinuity of circular shape. Then a similar force density on the disk is reproduced, adjusting the intensity in order to find a similar axial induced velocity on the disk. The results are compared in a steady state, which means simply taking $\omega = 0$ in Huang and Peters model, while we have to run a simulation and to wait for it to stabilize in the case of the new model. Without the mass flow parameter extension, Huang and Peters model behaves as if the free stream velocity was much higher than the induced velocity, therefore

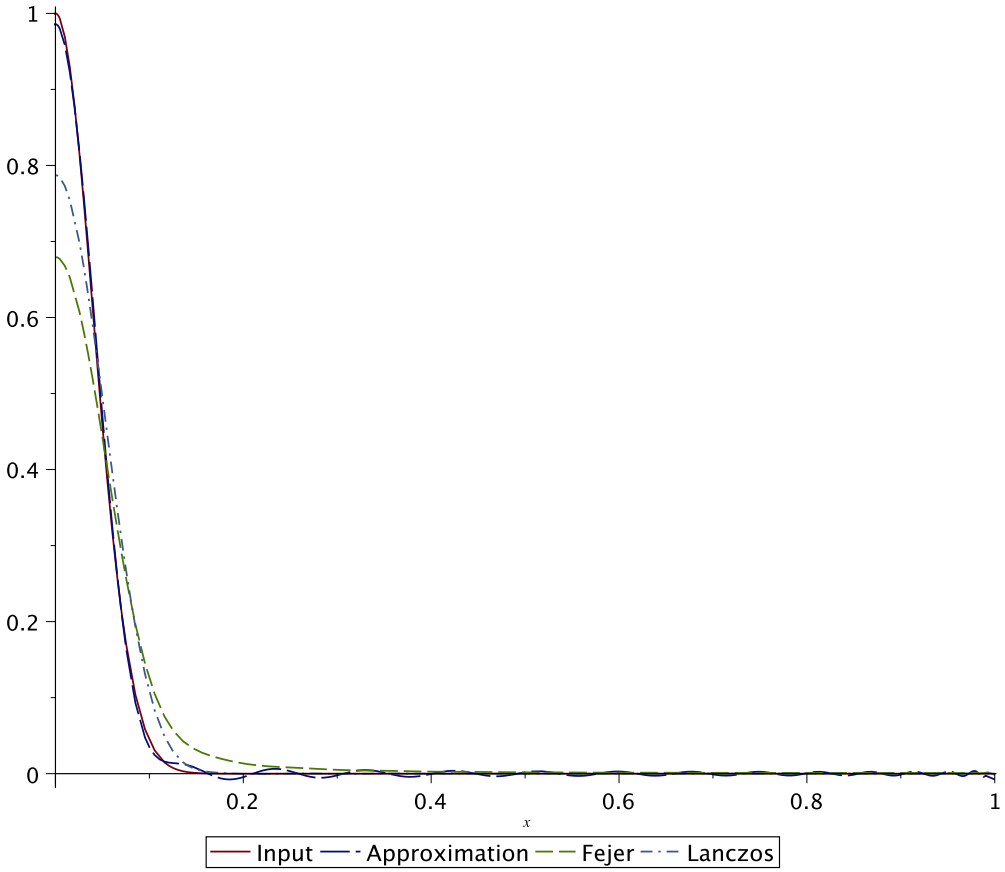

Figure 2: Comparison of Fejer and Lanczos filters on the polynomial approximation of a gaussian function by the γ_n polynomials on $[0, 1]$ with 60 elements

the comparison is done by using a consequent free stream velocity.

A summary of the conditions used for both model can be found in Table 1. The nomenclature used in this table is the same as the one found in Ref [1, 14]. It is also interesting to notice that, although the number of elements used in our case is one order of magnitude higher than the one used in the case of Huang and Peters model, the size of the matrices is smaller.

On Fig. 3 and Fig. 4, one can see that both models predict the same order of magnitude of both the axial and radial induced velocities. The main differences occur at the edge of the disk that are caused by the differences between both visions of the rotor. Furthermore, only an axial force density is applied, while the discontinuity of pressure does also act in the other directions. This could explain the differences between the two models on the radial velocity.

5.2. Extreme flight conditions

In this section we present results obtained for flight conditions that are not in the validity domain of the Huang and Peters model. The first example of such conditions is the high descending rate case. Here the fact that the velocity potential assumption is taken invalidates the possibility of having part of the wake on both side of the rotor. Figure 5 shows the velocity field around a uniformly loaded rotor added to the free stream. It shows that the new proposed model was able to reproduce the wake above the rotor as would be expected in such a case.

5.3. Transition flight

One issue that the Huang and Peters model encounters is its difficulties to render smoothly the variations of the wake during the transition from one flight condition to another. This is mainly due to the linearization of the equations. The rotor wake distortion during maneuvering flight has however an important impact on the accurate prediction of the flight dynamics of an helicopter, most notably on the

Huang and Peters Model		New Model	
Inputs as pressure discontinuity	τ_0^1	Force density sources	$\sqrt{1-(x+1)^2}$ for $x \in [-1, 0]$
Number of elements	$m_{odd} = 20$, $m_{even} = 10$, Total: 157	Number of elements	$N_r = 50$, $N_j = 50$, $N_\theta = 1$, Total: 2500
Conditions	$\omega = 0, \chi = 0$	Conditions	$V_\infty = 0.5$, $\Lambda = 5$, $\delta_t = 2E - 3$
		Filter order	$p = 20$

Table 1: Input data for comparison with Huang and Peters model

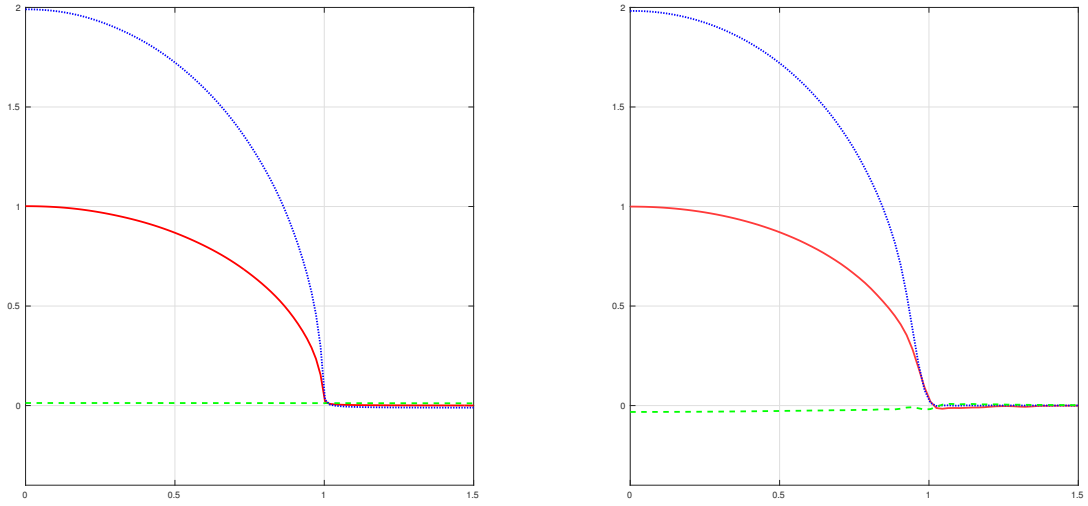

(a) Axial velocity given by Peters and Huang's model

(b) Axial velocity given by the present model

Figure 3: Comparison of the axial velocity between Peters and Huang's model and the present model for a τ_0^1 load, as presented in [1]. The green dashed line is taken $2R$ above the rotor, the red continuous one on the disk, and the blue dotted one $2R$ below the disk

off-axis response, as shown in Ref [22]. Zhao, Prasad and Peters have in particular worked on modelling a curved wake using several stream tubes, in Ref. [23], in order to capture this effect. Here the capabilities of the new model are demonstrated on a theoretical case of transition between hover and forward flight. A uniform load is applied to the rotor in hover conditions. Once the wake has developed in the domain, a constant forward velocity is instantaneously applied to the rotor. Figure 6 represents the evolution of the wake in those conditions. This underlines the benefits of taking no assumptions on the shape of the rotor wake and streamlines. Yet, one can see on Fig 6 (f) that the velocities leaving the domain on the right of the domain generate non physical velocities at the left of the domain. This is due to the low number of states used to describe the azimuthal coordinate which leads to a Gibbs phenomenon on the border of the domain.

5.4. Comparison with a prescribed wake model

In order to compare the results of this new model with a prescribed wake model, we have coupled it with a blade element model. An isolated blade of the 7AD rotor is used, rotating at $\Omega = 1020$ rpm, and ascending at $V_\infty = 5.0 m/s$.

Figure 8 shows the comparison between the axial induced velocity given by both model. It shows a good agreement, both in the shape of the distribution and in its amplitude, with the exception of the very tip of the blade, which has a less precise representation because of the high gradients it experienced, which are more difficult to represent. As

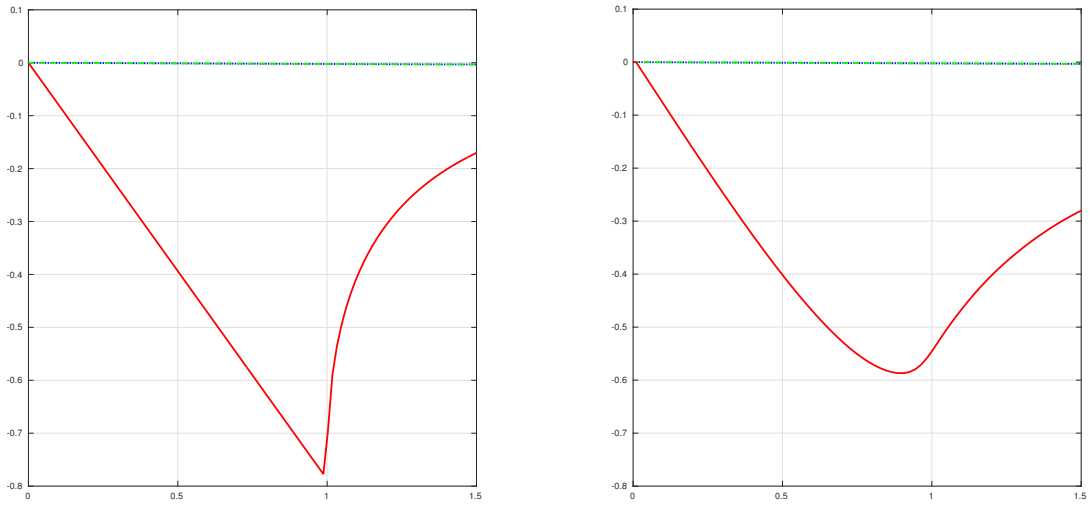

(a) Radial velocity given by Peters and Huang's model

(b) Radial velocity given by the present model

Figure 4: Comparison of the radial velocity between Peters and Huang's model and the present model for a τ_0^1 load, as presented in [1]. The green dashed line is taken $2R$ above the rotor, the red continuous one on the disk, and the blue dotted one $2R$ below the disk

a consequence the force distribution on the blade is also well represented, as can be seen on Fig. 7. However, the radial and the orthoradial component of the velocity are not as well described. Figure 9 shows a decent agreement of the tendencies of the radial velocity, although the amplitude does not match, but Fig. 10 shows a great difference between both models. This might be explained by the fact that the forces that the new model take into account are, here, only the axial forces, and it therefore lack the representation that a circulation source term could give. Further investigations are needed to properly understand and explain this discrepancy.

6. CONCLUSIONS

This paper presents a new model of rotor induced velocities based on the incompressible Euler equations with no further assumptions. The capacities of this new model have been illustrated on several test cases and compared to the Huang and Peters model [14], as well as with a prescribed wake model.

Its main advantages are that the rotor induced flow field is described as a whole in a homogeneous way, (thus without requiring the blending of several different models through the use of transition factors); that there is no potential flow assumption, the fundamental conservation laws governing the airflow are respected intrinsically, for example the continuity equation is embedded into the model providing a natural respect of the radial contraction of the rotor wake; that there is no linearization of the convection terms in the momentum conservation equation, therefore the shape of the rotor wake and streamlines is free and varies dynamically with the flight conditions and inputs allowing the model to captures the wake transition and distortion.

Although it is not deprived of flaws which can be solved by further developments, it is thought that this new model is a significant step towards a generation of fast, accurate and versatile models of rotor induced velocities.

7. ACKNOWLEDGMENTS

The first author would like to acknowledge the financial support provided by ONERA and region PACA in the development of this work.

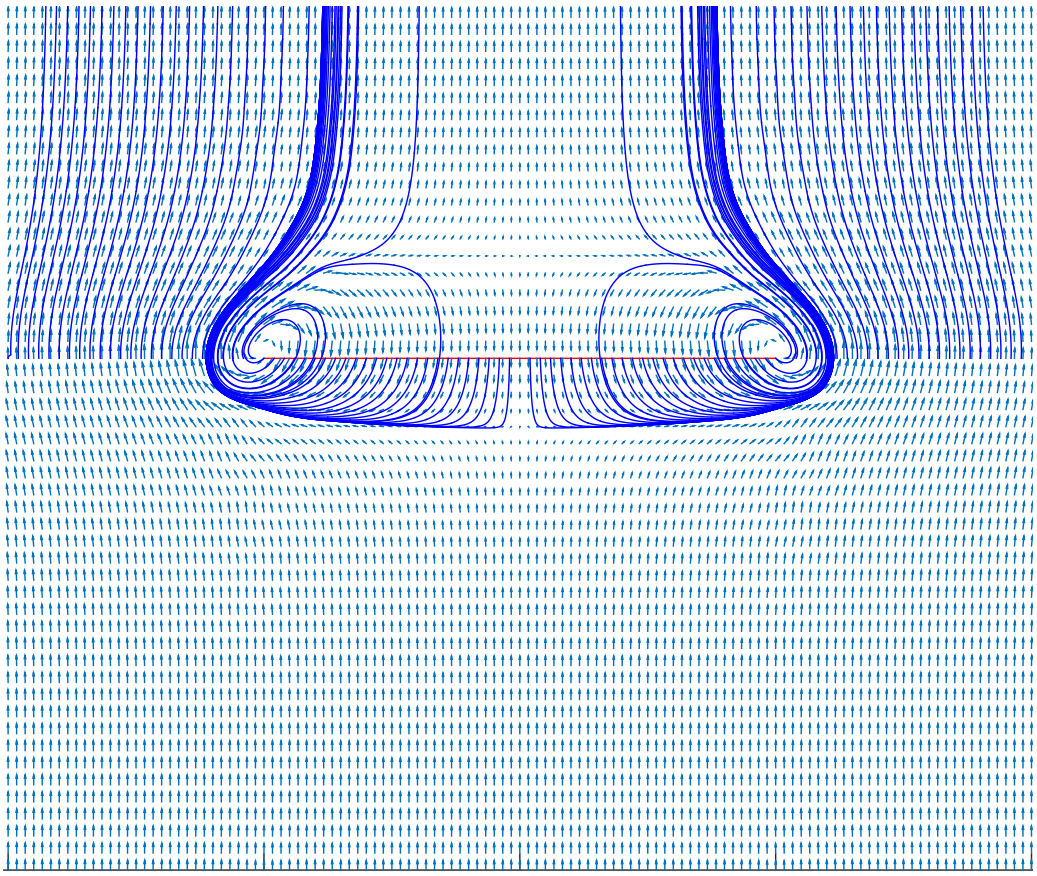

Figure 5: Induced velocity and free stream velocity in the case of a descending rotor.
The red line represents the rotor, and the blue lines represent the streamlines emanating from the rotor disk plane with the new proposed model.

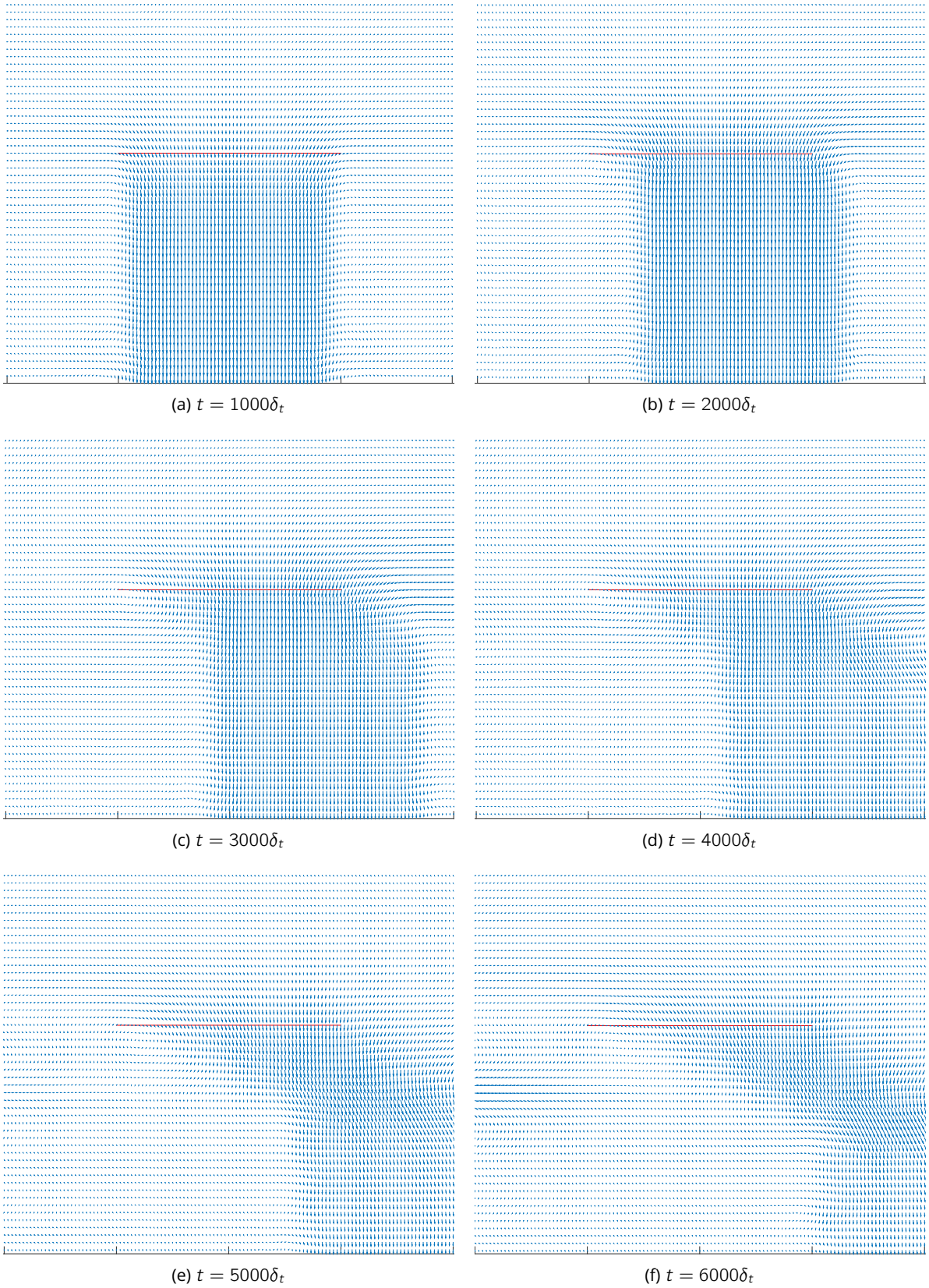

(a) $t = 1000\delta_t$ (b) $t = 2000\delta_t$

(c) $t = 3000\delta_t$ (d) $t = 4000\delta_t$

(e) $t = 5000\delta_t$ (f) $t = 6000\delta_t$

Figure 6: Evolution of the induced velocities in the $y = 0$ plane, with $N_r = 30$, $N_j = 30$ and $N_\theta = 20$.

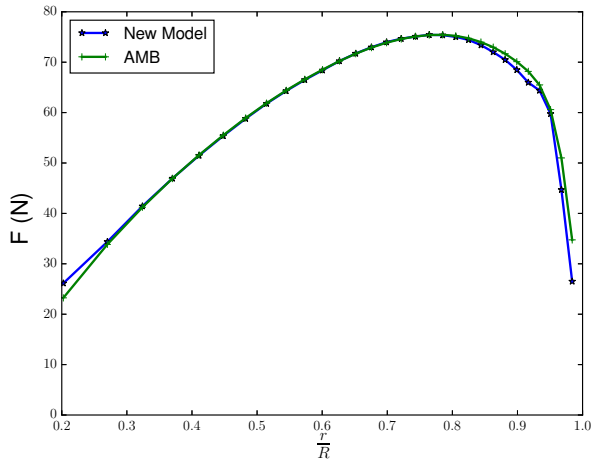

Figure 7: Comparison of the lift generated between the new model
and a prescribed wake model (AMB)

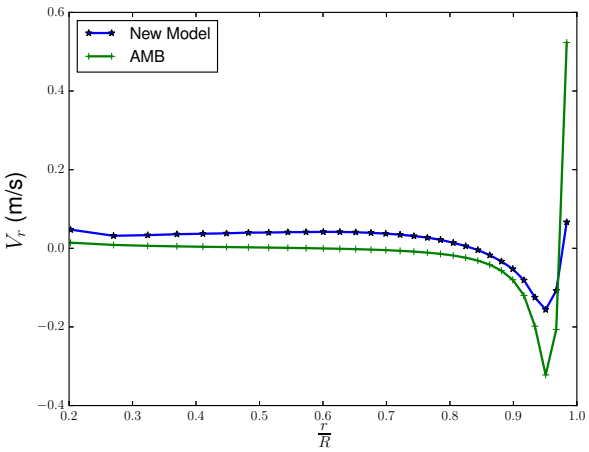

Figure 9: Comparison of the radial induced velocity between the new model
and a prescribed wake model (AMB)

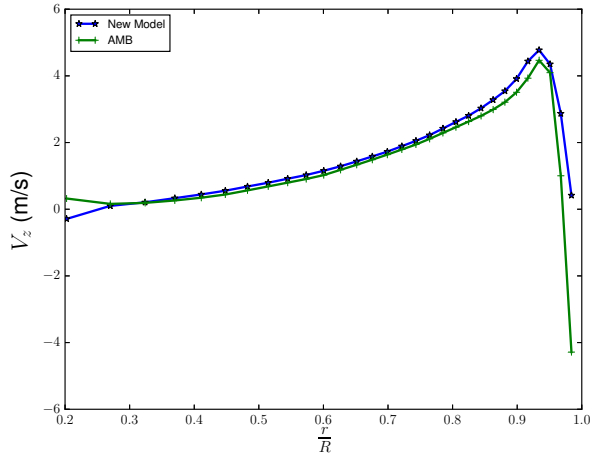

Figure 8: Comparison of the axial induced velocity between the new model
and a prescribed wake model (AMB)

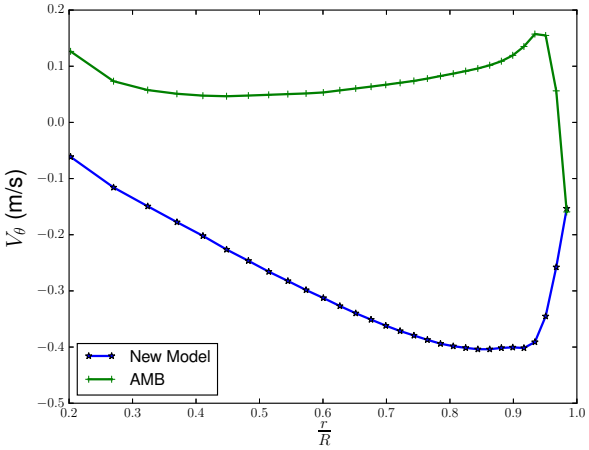

Figure 10: Comparison of the orthoradial induced velocity between the new model
and a prescribed wake model (AMB)

REFERENCES

[1] Jianzhe Huang, David A Peters, and JVR Prasad. "Converged Velocity Field for Rotors by a Blended Potential Flow Method". In: *GSTF Journal on Aviation Technology (JAT)* 1.2 (2015).

[2] Kenneth B Amer. "Theory of helicopter damping in pitch or roll and a comparison with flight measurements". In: *NACA TN-2136* (1950).

[3] Dale M Pitt and David A Peters. "Theoretical prediction of dynamic-inflow derivatives". In: *Vertica* 5 (1980), pp. 21–34.

[4] John T Conway. "Analytical solutions for the actuator disk with variable radial distribution of load". In: *Journal of Fluid Mechanics* 297 (1995), pp. 327–355.

[5] Frederic Le Chuiton. "Actuator disc modelling for helicopter rotors". In: *Aerospace Science and Technology* 8.4 (2004), pp. 285–297.

[6] David O'Brien and Marilyn Smith. "Analysis of rotor-fuselage interactions using various rotor models". In: *43rd AIAA Aerospace Sciences Meeting and Exhibit*. 2005, p. 468.

[7] David A Peters. "How dynamic inflow survives in the competitive world of rotorcraft aerodynamics". In: *Journal of the American Helicopter Society* 54.1 (2009), pp. 11001–11001.

[8] JM Lopez, F Marques, and Jie Shen. "An efficient spectral-projection method for the Navier–Stokes equations in cylindrical geometries: II. Three-dimensional cases". In: *Journal of Computational Physics* 176.2 (2002), pp. 384–401.

[9] H Ralph Lewis and Paul M Bellan. "Physical constraints on the coefficients of Fourier expansions in cylindrical coordinates". In: *Journal of Mathematical Physics* 31.11 (1990), pp. 2592–2596.

[10] F Domenichini and B Baccani. "A formulation of Navier–Stokes problem in cylindrical coordinates applied to the 3D entry jet in a duct". In: *Journal of Computational Physics* 200.1 (2004), pp. 177–191.

[11] JM Lopez and Jie Shen. "An efficient spectral-projection method for the Navier–Stokes equations in cylindrical geometries: I. Axisymmetric cases". In: *Journal of Computational Physics* 139.2 (1998), pp. 308–326.

[12] Suchuan Dong and Jie Shen. "A pressure correction scheme for generalized form of energy-stable open boundary conditions for incompressible flows". In: *Journal of Computational Physics* 291 (2015), pp. 254–278.

[13] Jie Shen. "Efficient spectral-Galerkin methods III: Polar and cylindrical geometries". In: *SIAM Journal on Scientific Computing* 18.6 (1997), pp. 1583–1604.

[14] Jianzhe Huang. *Potential-flow Inflow Model Including Wake Distortion and Contraction*. Doctor of Science Dissertation, Washington University in St. Louis, 2015.

[15] Chengjian He, CS Lee, and Weibin Chen. "Finite state induced flow model in vortex ring state". In: *Journal of the American Helicopter Society* 45.4 (2000), pp. 318–320.

[16] Jorge A Morillo and David A Peters. "Velocity field above a rotor disk by a new dynamic inflow model". In: *Journal of aircraft* 39.5 (2002), pp. 731–738.

[17] JC Simo and F Armero. "Unconditional stability and long-term behavior of transient algorithms for the incompressible Navier-Stokes and Euler equations". In: *Computer Methods in Applied Mechanics and Engineering* 111.1-2 (1994), pp. 111–154.

[18] Hervé Vandeven. "Family of spectral filters for discontinuous problems". In: *Journal of Scientific Computing* 6.2 (1991), pp. 159–192.

[19] David Gottlieb and Jan S Hesthaven. "Spectral methods for hyperbolic problems". In: *Partial Differential Equations*. Elsevier, 2001, pp. 83–131.

[20] Jan Hesthaven and Robert Kirby. "Filtering in Legendre spectral methods". In: *Mathematics of Computation* 77.263 (2008), pp. 1425–1452.

[21] Alex Kanevsky, Mark H Carpenter, and Jan S Hesthaven. "Time-consistent filtering in spectral and spectral element methods". In: *J. Comput. Phys., submitted for publication* (2004).

[22] PM Basset and F Tchen-Fo. "Study of the rotor wake distortion effects on the helicopter pitch-roll cross-couplings". In: *European Rotorcraft Forum*. Vol. 24. Associazione Italiana di Aeronautica ed Astronautica. 1998, FM06–FM06.

[23] Jinggen Zhao, JVR Prasad, and David A Peters. "Rotor dynamic wake distortion model for helicopter maneuvering flight". In: *Journal of the American Helicopter Society* 49.4 (2004), pp. 414–424.